ChemPubSoc Europe

DOI: 10.1002/chem.201600214

CHEMISTRY A European Journal Full Paper

Electrochemistry |*Hot Paper*|

Carbon-Nanotube-Mediated Electrochemical Transition in a Redox-Active Supramolecular Hydrogel Derived from Viologen and an L-Alanine-Based Amphiphile

Sougata Datta[a, b] and Santanu Bhattacharya*[a, b, c]

Abstract: A two-component hydrogelator **(16-A)$_2$-V^{2+}**, comprising an L-alanine-based amphiphile (**16-A**) and a redox-active viologen based partner (**V^{2+}**), is reported. The formation the hydrogel depended, not only on the acid-to-amine stoichiometric ratio, but on the choice of the L-amino acid group and also on the hydrocarbon chain length of the amphiphilic component. The redox responsive property and the electrochemical behavior of this two-component system were further examined by step-wise chemical and electrochemical reduction of the viologen nucleus (V^{2+}/V^{+} and V^{+}/V^{0}). The half-wave reduction potentials ($E_{1/2}$) associated with the viologen ring shifted to more negative values with increasing amine component. This indicates that higher extent of salt formation hinders reduction of the viologen moiety. Interestingly, the incorporation of single-walled carbon nanotubes in the electrochemically irreversible hydrogel **(16-A)$_2$-V^{2+}** transformed it into a quasi-reversible electrochemical system.

Introduction

Realization of the importance of weak, noncovalent interactions has spurred widespread efforts towards the evolution of molecular systems endowed with new properties and functions based on the principles of self-assembly.[1] A wide range of materials that have potential applications in daily life, industry, and various fields, including nanotechnology,[2] biomaterials,[3] stimuli-responsive systems,[4] and in catalysis[5] and so forth have come out of these efforts. Among these, the self-assembly of low-molecular-weight gelators (LMWGs) is a subject of increasing interest, because this strategy allows the formation of various self-assembled architectures (i.e., helical and bundles of fibers of high aspect ratio,[6] ribbons,[7] rings,[8] tubules,[9] etc.). LMWGs include a wide variety of molecular entities, for example, long-chain hydro- and fluorocarbon or steroid derivatives,[10] amino-acid analogs,[11] ureas,[12] carbohydrate-derived systems,[13] charge-transfer complexes,[14] and organic salts,[15] and so on.

Attachment of a stimuli-inducible functional group at the molecular level, may act as a "switch" for monitoring the growth and demolition of the effects of self-assembly in a reversible manner. Several attempts have been made to obtain various LMWGs with stimuli-responsive properties, reacting to stimuli, such as, heat,[16] ultrasound,[17] light,[18] pH,[19] redox activity,[20] enzymatic manipulation,[21] host–guest interaction,[22] and external additives.[23] In this context redox-active LMWGs, which form an imperative part of the stimuli-responsive LMWGs, have attracted recent attention. This is because of the possibility to achieve control over physical and/or chemical properties, that is, morphology (i.e., size and shape), surface properties, conductivity, color, or solubility in a reversible manner by shifting between the redox states.[24]

Gel-to-sol transition processes associated with the chemical and electrochemical reactions of various redox-active LMWGs, for example, tetrathiafulvalene (TTF) derivatives[25] and organometallic complexes,[26] especially ferrocene[27]-based compounds, have been extensively investigated. Xu and co-workers have reported a tripeptide-derived metallo-hydrogelator that, not only self-assembles to form a hydrogel, but also exhibits gel-to-sol transition upon oxidation of the metal center. Interestingly, the nanofibers resulting from the self-assembly of the hydrogelator have the width of a single molecule of the hydrogelator.[28] Zhang and co-workers discovered a structurally simple, stimuli-responsive hydrogelator based on ferrocene and L-phenylalanine.[29] These authors showed the utility of the hydrogel in the mobilization of fragile enzymes by cyclic voltammetry experiment.[29b] Recently, Adams and Cameron have explored a method for the electropolymerization of low-molecular-weight hydrogelators derived from carbazole-protected amino acids to form polymers with unique structures.[30] This opens the possibility of using partially or completely polymerized hydrogels for a range of sensing and bioelectronics applications. Thus, insertion of a redox-active moiety often offers

[a] *Dr. S. Datta, Prof. Dr. S. Bhattacharya*
Department of Organic Chemistry, Indian Institute of Science
Bangalore 560012, Karnataka (India)
E-mail: sb@orgchem.iisc.ernet.in

[b] *Dr. S. Datta, Prof. Dr. S. Bhattacharya*
Present address: Director's Research Unit (DRU)
Indian Association for the Cultivation of Science
Jadavpur, Kolkata 700 032 (India)

[c] *Prof. Dr. S. Bhattacharya*
Jawaharlal Nehru Centre for Advanced Scientific Research
Bangalore 560 064, Jakkur (India)

Supporting information for this article can be found under http://dx.doi.org/10.1002/chem.201600214.

the corresponding LMWGs attractive electro-active and chemo-responsive properties to tune the gel-to-sol transition by oxidation/reduction processes, as well as though reactions with electron donors/acceptors.

4,4′-Bipyridinium (viologen) derivatives are well-known redox systems (V^{2+}) capable of showing two successive reductive processes, which are both chemically and electrochemically reversible.[31] The first reductive step results in the formation of an intensely blue-colored radical cation species, which, upon further reduction, forms a yellow-colored, neutral quinoid moiety.[31] There are only a handful of reports of viologen-derived gels.[32] George and co-workers reported co-assembly of a noncovalent, donor–acceptor amphiphilic pair of coronene and viologen derivative, which transformed into cylindrical micelles to the generate hydrogel.[32c]

Single-walled carbon nanotubes (SWNT) have been modified extensively in the last few years in either a covalent or noncovalent manner, because of a lack of solubility in water and in various organic media. Covalent modification at the sidewalls of SWNTs by attaching hydrophilic functional groups renders them water dispersible. However, this results in serious alteration of the electronic structure of the SWNTs by disruption of the network of sp^2-hybridized carbons.[33] An alternative strategy to achieve solubilization of SWNTs in water is though noncovalent wrapping of the SWNTs by using hydrophilic polymers[34]/biomolecules[35]/small amphiphilic molecules[36] and so forth. Fukushima et al. showed transparent gel formation by mixing an imidazolium-type, room-temperature ionic liquid with SWNTs.[37] We developed a gel–SWNT nanocomposite from SWNTs and an organogelator based on a fatty acid amide with limited dispersion ability.[38] The efficiency of incorporation of SWNTs can be improved further by extending this idea to a luminescent organogel system made of conjugated oligo-*p*-phenylenevinylenes.[39]

Herein, we introduce an ion-pair, two-component system, which is capable of immobilizing water, leading to hydrogelation. The dicarboxylic-acid part of viologen imparts a redox-active character (Scheme 1). Appendage of L-alanine though a long-chain amide connector allows formation of an extensive hydrogen-bonded network in the assemblies, where the hydrocarbon chain introduces van der Waals interactions. Also in place of L-alanine, L-phenylalanine is introduced to investigate the influence of charge-transfer (CT) interactions, if any, between the phenyl and the viologen ring in the gelation process. The mechanism of the systematic growth of the supramolecular assembly is investigated by small-angle X-ray diffraction (SAXD) analysis. The effect of variation of the acid-to-amine stoichiometric ratio on the gelation process is examined by FT-IR, ^{1}H NMR spectroscopy, electron microscopy, and rheological studies. Because of the amphiphilic nature of the molecule, SWNTs can be dispersed effectively in the two-component hydrogel. Electrochemical activity of the hydrogel and the resulting SWNTs–hydrogel nanocomposite is analyzed by cyclic voltammetry.

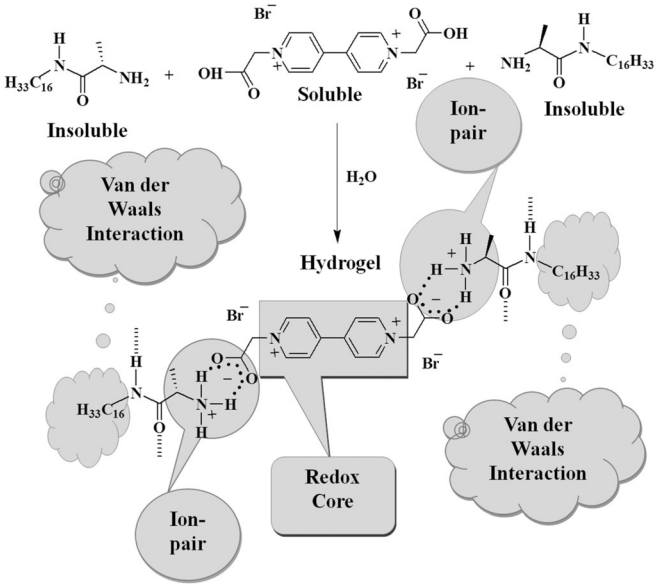

Scheme 1. Molecular representation of redox-active and salt-type hydrogelator, **(16-A)$_2$-V^{2+}** and a schematic illustration of the associated two-component hydrogelation process.

Results and Discussion

Synthesis

Compounds **1** and **2a–f** (Figure 1a) were synthesized according to Scheme S1 in the Supporting Information and were characterized by ^{1}H NMR, ^{13}C NMR spectroscopy, FT-IR spectroscopy, and mass spectrometry (ESI-MS; see the Experimental Section in the Supporting Information).

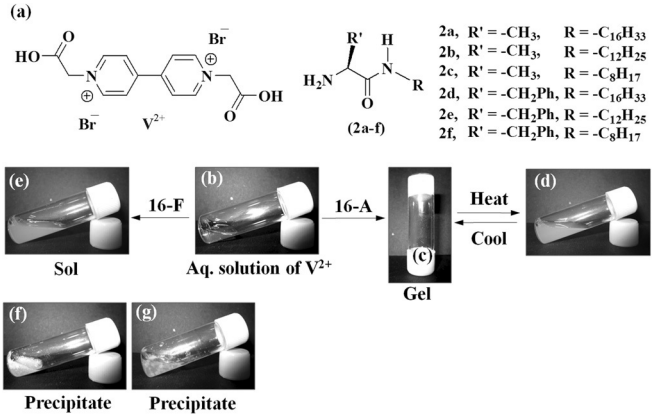

Figure 1. (a) Molecular structures of **V^{2+}** and **2a–f** (***n*-A** and ***n*-F**, where $n = 8$, 12 and 16). Photographs of (b) an aqueous solution of **V^{2+}**, (c, d) thermo-reversible hydrogels of 1:2 mixtures of **V^{2+}** and **16-A**, (e) a viscoelastic sol of a 1:2 mixture of **V^{2+}** and **16-F**, and (f, g) precipitates of **16-A** and **16-F**, respectively, in water (pH ca. 6.9).

Gelation studies

Compound **V^{2+}** was checked for gelation in water in the presence of L-alanine or L-phenylalanine amides of aliphatic

amines (**2a–f**) of various hydrocarbon chain lengths (Figure 1a). It was observed that long-chain C_8 (**8-A**) and C_{12} (**12-A**) amine derivatives of L-alanine formed turbid solutions in the presence of $\mathbf{V^{2+}}$ in water, but never gels, not even upon prolonged aging or sonication. Only the C_{16} amine derivative of L-alanine (**16-A**) was capable of forming stable hydrogels at appropriate acid ($\mathbf{V^{2+}}$)-to-amine (**16-A**) ratio on standing for 15–20 min at room temperature. These hydrogels transformed to apparent solutions upon heating at 60 °C. Gelation characteristics of various salt-type mixtures are listed in the Table S1 in the Supporting Information. A 1:1 mixture of dicarboxylic acid ($\mathbf{V^{2+}}$) and amine (**16-A**) could not induce gelation. However, the 1:1.5 and 1:2 stoichiometric ratios of the acid ($\mathbf{V^{2+}}$)-to-amine (**16-A**) mixtures readily formed opaque and thermo-reversible hydrogels (Figure 1c and d). Lowest minimum gelator concentration (mgc) was observed with the $\mathbf{(16\text{-}A)_2\text{-}V^{2+}}$ ([$\mathbf{V^{2+}}$] = 11.5 mM = mgc, [**16-A**] = 23 mM). Addition of excess amine (**16-A**) resulted in leaching of solvents and disruption of the gelation process. Interestingly, aliphatic-chain (C_8, C_{12} and C_{16})-appended L-phenylalanine derivatives (***n*-F**, where $n = 8$, 12, and 16) afforded clear viscoelastic fluids, which however, did not gelate, under similar conditions even after standing for a long time at room temperature (Figure 1e).

It is important to note that each of these L-alanine (***n*-A**) and L-phenylalanine (***n*-F**) derivatives is insoluble in water on their own (Figure 1f and g), whereas $\mathbf{V^{2+}}$ is water soluble without any additives (Figure 1b). However, the presence of $\mathbf{V^{2+}}$ in ***n*-A** or ***n*-F** sols rendered the resulting mixture water-dispersible on heating followed by brief sonication; presumably due to salt formation. Presence of L-phenylalanine in the mixture was expected to induce precipitation instead of solubilization due to greater hydrophobicity of the phenyl ring relative to that of the methyl group of L-alanine. Solubilization of L-phenylalanine derivatives (***n*-F**) in the presence of $\mathbf{V^{2+}}$ might be a result of charge-transfer (CT) interactions between the phenyl residue and the viologen ring. This phenomenon is discussed in detail below (^{1}H NMR study). Addition of two equivalents of palmitic acid or stearic acid instead of **16-A** to the aqueous solution of $\mathbf{V^{2+}}$ did not lead to gelation. This result clearly suggests the importance of the amide linkage in the inter-molecular assembly of gelator molecules, leading to gelation. The effect of various salts on the gelation process was also investigated. Interestingly, addition of various acetate salts of Na^+, Cd^{2+}, Mg^{2+}, Ni^{2+}, Co^{2+}, Zn^{2+}, Cu^{2+}, Mn^{2+} did not disrupt the gelation process. On the other hand, the integrity of the gel also remained unaltered in the presence of various Na^+ or Cu^{2+} salts with counteranions, such as, Cl^-, Br^-, NO_3^-, and citrate.

^{1}H NMR study

Figure 2a shows ^{1}H NMR spectra of $\mathbf{(16\text{-}A)_n\text{-}V^{2+}}$ in D_2O at 25 °C at various stoichiometries of **16-A** ($n = 0.5$, 1, 1.5, and 2). The ^{1}H NMR signal at 5.4 ppm of $\mathbf{V^{2+}}$ was assigned to the methylene protons attached to the –COOH group; these showed significant upfield shifts upon increasing the amine (**16-A**) content. This may be interpreted by an increase in the extent of carboxylate anion formation with increasing the amine (**16-A**)-to-acid ($\mathbf{V^{2+}}$) stoichiometric ratio. The ^{1}H NMR signal appeared to be quite broad due to the gel formation as the acid ($\mathbf{V^{2+}}$)-to-amine (**16-A**) stoichiometric ratio reached approximately 1:2. To understand the reason for formation of viscoelastic fluids from L-phenylalanine derivatives in the presence of $\mathbf{V^{2+}}$, ^{1}H NMR spectra of $\mathbf{(16\text{-}F)_n\text{-}V^{2+}}$ in D_2O at 25 °C were recorded at various stoichiometries of **16-F** ($n = 0.5$, 1, 1.5, and 2). Similarly to above, the ^{1}H NMR signal at 5.4 ppm shifted upfield due to the salt formation. But, no significant line broadening occurred with the addition of **16-F** (Figure 2c). This indicates an isotropic distribution of molecules in the sol state, thereby averaging out or minimizing the dipolar interactions between the proton nuclei. Hence, salt formation is the common characteristic of gel of $\mathbf{(16\text{-}A)_2\text{-}V^{2+}}$ and sol of $\mathbf{(16\text{-}F)_2\text{-}V^{2+}}$.

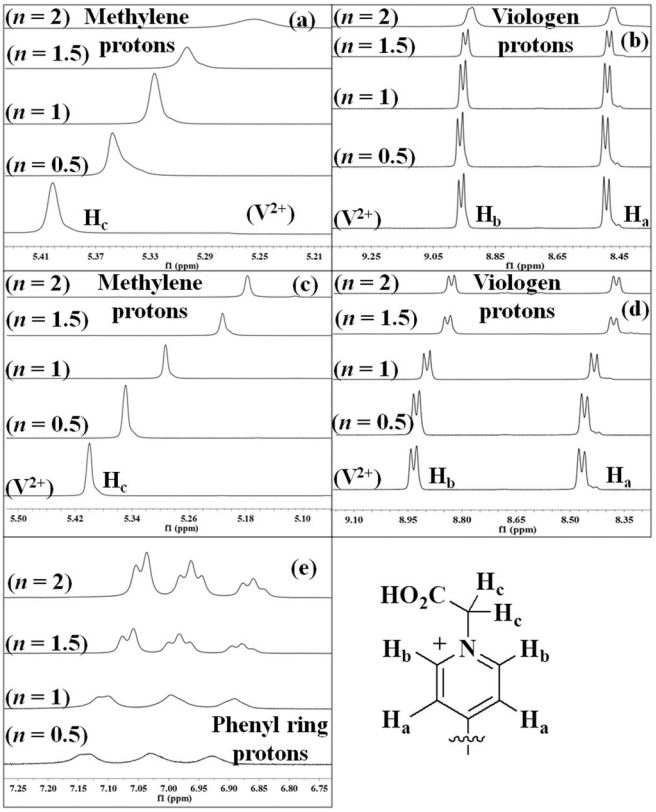

Figure 2. Stoichiometry-dependent partial ^{1}H NMR spectra of (a, b) $\mathbf{(16\text{-}A)_n\text{-}V^{2+}}$ and (c–e) $\mathbf{(16\text{-}F)_n\text{-}V^{2+}}$ in D_2O at 25 °C, $n = 0.5$, 1, 1.5 and 2. Concentration of $\mathbf{V^{2+}}$ is 11.5 mM in all cases.

In addition to salt formation, the significantly different ^{1}H NMR spectra of $\mathbf{(16\text{-}F)_n\text{-}V^{2+}}$ in D_2O compared with that of $\mathbf{(16\text{-}A)_n\text{-}V^{2+}}$ was probably also due to the CT from phenyl to viologen rings. Phenyl-ring protons appeared in the range of 6.9–7.2 ppm, whereas, the ^{1}H NMR signals at 8.46 and 8.93 ppm were assigned to the ^{1}H nuclei of the viologen rings in $\mathbf{V^{2+}}$. Each of these signals shifted upfield with increasing **16-F** content, suggesting a face-to-face stacking, involving the donor and acceptor molecules (Figure 2d and e).[32c] Thus, the aromatic π electrons of the phenyl ring induced shielding of the viologen-ring protons. At the same time, phenyl-ring pro-

tons exhibited a small upfield shift. Interestingly, the ^{1}H NMR signals associated with the viologen-ring protons did not show any significant shift with the increase of the **16-A**/$\mathbf{V^{2+}}$ stoichiometric ratio (Figure 2b). This clearly suggests that CT is the probable origin of the mechanism of sol formation of $\mathbf{(16\text{-}F)_2\text{-}V^{2+}}$. This is further supported by UV/Vis spectroscopy. A weak absorption band was observed in the range of 450–500 nm (Figure S1 in the Supporting Information) in case of $\mathbf{(16\text{-}F)_n\text{-}V^{2+}}$ at various stoichiometries, indicating CT interaction between the donor (**16-A**) and the acceptor molecules ($\mathbf{V^{2+}}$).[40]

FT-IR spectroscopy

FT-IR spectral analysis of $\mathbf{V^{2+}}$ and $\mathbf{(16\text{-}A)_n\text{-}V^{2+}}$ at various stoichiometries ($n = 0.5$, 1 and 2) was performed to confirm that salt formation was involved in the sol-to-gel transition process; in other words, that electrostatic interactions are crucial for the self-assembly. Figure S2 (see the Supporting Information) shows FT-IR spectra of $\mathbf{V^{2+}}$ and $\mathbf{(16\text{-}A)_n\text{-}V^{2+}}$ at various acid ($\mathbf{V^{2+}}$)-to-amine (**16-A**) ratio. The IR band at 1742 cm^{-1} in the FT-IR spectra of $\mathbf{V^{2+}}$ is assigned to the COOH group, which has almost disappeared in the FT-IR spectra of $\mathbf{(16\text{-}A)_2\text{-}V^{2+}}$. Additionally, a new shoulder appeared at 1669 cm^{-1}, which indicated generation of a COO^- anion, due to the salt formation.[41]

Morphological features and structural analysis

Scanning electron microscopy (SEM) images provide a possible mechanistic insight to the growth of the supramolecular assembly with an increased amine (**16-A**) proportion. Lower concentration of amine (**16-A**) in the salt-type mixture showed existence of aggregated organizations (Figure S3 in the Supporting Information). But tape-like fibrous network with diameters ranging from 10–30 μm was clearly observed in the xerogel of $\mathbf{(16\text{-}A)_2\text{-}V^{2+}}$ (Figure 3a). The morphology of the freeze-dried gel of $\mathbf{(16\text{-}A)_2\text{-}V^{2+}}$ was further investigated by atomic force microscopy (AFM). Fibrous nanostructures of high aspect ratio with lengths >10–15 μm and uniform average diameters of 100–150 nm were observed (Figure 3b).

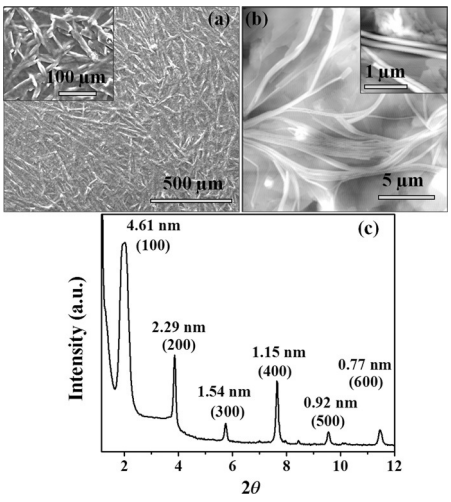

Figure 3. (a) SEM, (b) AFM images, and (c) SAXD plot of the xerogel derived from $\mathbf{(16\text{-}A)_2\text{-}V^{2+}}$.

The small-angle X-ray diffraction (SAXD) pattern of the xerogel of $\mathbf{(16\text{-}A)_2\text{-}V^{2+}}$ showed six peaks with *d*-spacings of 4.61, 2.29, 1.54, 1.15, 0.923, and 0.771 nm. These were observed with a *d*-spacing ratio of 1:1/2:1/3:1/4:1/5:1/6, indicating a lamellar pattern of the gel aggregates of $\mathbf{(16\text{-}A)_2\text{-}V^{2+}}$ with an interlayer spacing of 4.61 nm (Figure 3c).[6,16a]

Redox activity and cyclic voltammetry

To detect various redox states of the hydrogel, a layer of toluene was placed on the top of the hydrogel under an argon atmosphere (Figure 4a). This inhibits the quenching of the radical species by atmospheric oxygen, according to a published protocol.[31b] Careful injection of a freshly prepared aqueous solution of $NaBH_4$ (3 equiv) into the hydrogel phase (11.5 mM) resulted in the formation of a deep-blue-colored gel phase, possibly due to the formation of a viologen radical cation, accompanied by concomitant evolution of hydrogen gas.[31b] This phase was further converted into a yellow-colored sol due to the formation of fully reduced quinoid species after approximately 24 h and by this time a complete gel-to-sol transition had occurred (Figure 4a).

The above mentioned stepwise reduction processes were followed by UV/Vis spectroscopy (Figure S4 in the Supporting Information). Lee and co-workers have suggested that analogous yellow-colored quinoid species were generated due to reduction of the viologen derivatives, which phase transferred into the toluene layer because of the nonpolar character.[31b] However, we found the quinoid species in the aqueous layer. This indicates that the presence of dicarboxylic acid groups offers sufficient polarity to partition into the aqueous layer. We also used AFM to investigate the morphology of the aggregates present in the yellow sol generated after reduction with $NaBH_4$. This showed that the fibrous structure of $\mathbf{(16\text{-}A)_2\text{-}V^{2+}}$ transformed to a 'collapsed' aggregated structure due to a reduction-induced gel-to-sol transition (Figure S5 in the Supporting Information).

It may be instructive to compare the findings from other redox-active systems. Kaifer and co-workers synthesized various types of asymmetric redox-active dendrimers by integrating viologen or ferrocene and investigated rigorously by using electrochemical studies to mimic activities of redox-active proteins where the redox-active center was partially buried in the polypeptide backbone and located "off center" in the protein framework.[42] They also developed various synthetic water-soluble hosts in which redox-active guests were incorporated through host–guest interactions and investigated their properties to decipher intricate mechanistic details by considering them as models for enzyme-bound substrates.[43] Thus the presence of a redox-active moiety in a self-assembled matrix may be useful to sense the environment and provide critical information about the kinetics and thermodynamics associated with the mechanism and growth of the self-assembly. They first demonstrated that half-wave reduction potentials of the viologen core shifted to more negative values with increased

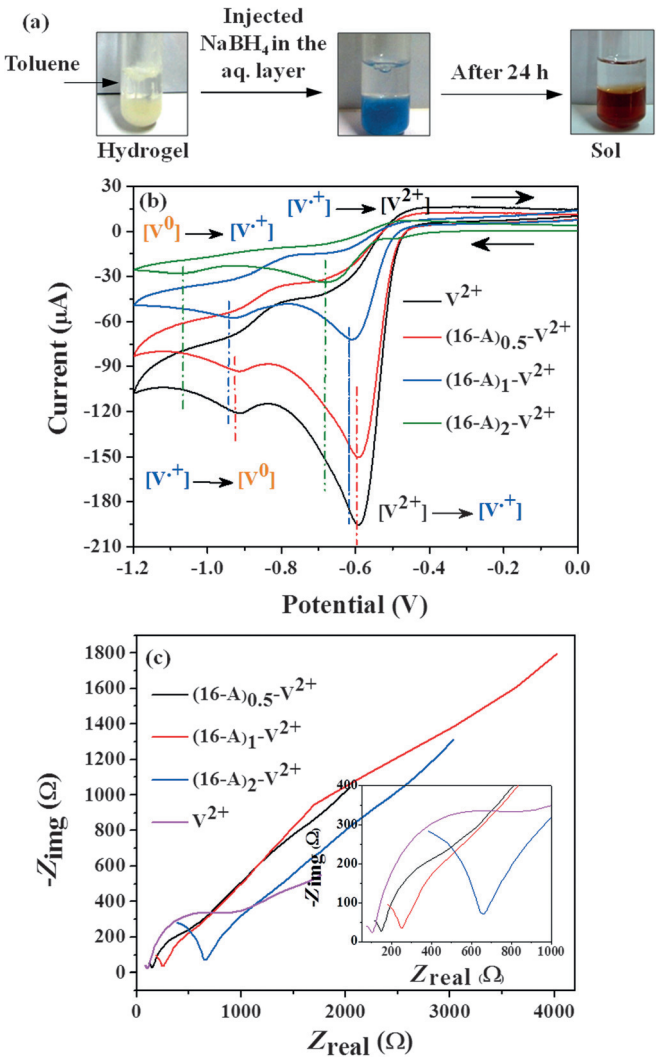

Figure 4. (a) Photographs showing the reduction of the viologen derivative, **(16-A)$_2$-V^{2+}** by $NaBH_4$. (b) Cyclic voltammetry responses of **(16-A)$_n$-V^{2+}** at various acid-to-amine stoichiometric ratios ($n = 0.5$, 1 and 2) in water on glassy carbon electrode in presence of LiCl (0.1 M) as the supporting electrolyte at a scan rate of 50 mV sec^{-1}. The concentration of **V^{2+}** is 11.5 mM in all cases (pH ca. 6.9). (c) Nyquist plots of **V^{2+}** and **(16-A)$_n$-V^{2+}** at various acid-to-amine stoichiometric ratios ($n = 0.5$, 1 and 2); Concentration of **V^{2+}** is 11.5 mM in all cases.

size of the Newkome-type dendrimers, thus indicating that there is a thermodynamic hindrance for the reduction process of dendrimers of higher molecular mass.[42] However, there is no report that investigates the mechanism of growth of supramolecular gelation processes by systematic electrochemical analysis.

Herein, we have developed a system with a redox-active viologen core, which is subjected to sense the supramolecular environment by following the redox properties as the acid (**V^{2+}**)-to-amine (**16-A**) stoichiometric ratio is varied. We recorded cyclic voltammograms of **(16-A)$_n$-V^{2+}** at various acid (**V^{2+}**)-to-amine (**16-A**) stoichiometries in presence of LiCl (0.1 M) as the supporting electrolyte (Figure 4b). **(16-A)$_n$-V^{2+}** exhibits the two consecutive one-electron reductions, as anticipated for any viologen compound. The cathodic scan clearly shows two distinguishable peaks associated with the two-step reduction processes. But poor peak current was observed in the anodic scan. This indicates that a very small amount of the reduced species was available to undergo oxidation in the anodic scan. Deviation from the reversibility is probably due to the instability of the reduced species. The irreversible electrochemical behavior of these various acid (**V^{2+}**)/amine (**16-A**) stoichiometric mixtures do not originate from the alkyl chains of (**16-A**); but rather from the intrinsic nature of the redox core (**V^{2+}**). The half-wave reduction potentials corresponding to the first reduction step of various acid (**V^{2+}**)/amine (**16-A**) stoichiometric mixtures are reported in Table S2 in the Supporting Information. Herein, we show a systematic growth of a hydrogel by successive increase of the amine (**16-A**) proportion. Figure 4b clearly shows that half-wave reduction potentials shift to more negative values with the growth of the supramolecular aggregate. Increased concentrations of the amine (**16-A**) induces more salt formation and increases the population of the amide group in the self-assembly. This results in increased polarity around the viologen moiety and hinders the reduction (loss of positive charge) of the viologen core. Hence, this behavior is quite similar to the behavior reported with the Newkome-type of dendrimers observed by Kaifer's group. Similar trends of negative shifts of the half-wave reduction potentials were also observed for samples that had been drop-coated on the glassy carbon electrode followed by careful drying.

Another interesting phenomenon was observed in the cyclic voltammetry studies. Peak current (i_p) associated with each of the half-wave reduction potentials monotonically decreased with the increase of amine (**16-A**) in **(16-A)$_n$-V^{2+}**. This finally reached a minimum at a 1:2 acid (**V^{2+}**)-to-amine (**16-A**) stoichiometric ratio [i_p(**V^{2+}**) > i_p($n = 0.5$) > i_p($n = 1$) > i_p($n = 2$)].

The peak current (i_p) is proportional to the square root of the diffusion coefficient (D) as described by the Randles–Sevcik equation [Eq. (1)]:[42]

$$i_p = 0.4463\, nFAC\,(nFvD/RT)^{1/2} \quad (1)$$

In this equation, n is the number of electrons appearing in half-reaction for the redox couple; v is the rate at which the potential is swept (V sec^{-1}); F is the Faraday's constant (96485 C mol^{-1}); A is the electrode area (cm^2); R is the universal gas constant (8.314 J mol^{-1} K); T is the absolute temperature (K); D is the diffusion coefficient of the analyte (cm^2 sec^{-1}); C is the concentration.

If the temperature is at 25 °C (298.15 K), the Equation (1) can be rewritten in a more concise form as:

$$i_p = (2.687 \times 10^5) n^{3/2} v^{1/2} D^{1/2} AC \quad (2)$$

We calculated the diffusion coefficients of various salt-type mixtures ($n = 0.5$, 1, and 2) associated with the first half-wave reduction potential by using Equation (2); these are listed in Table S3 in the Supporting Information ($n = 1$, $A = 0.09$ cm^2, $C = 0.0115 \times 10^{-3}$ mol cm^{-3}, $v = 50 \times 10^{-3}$ V s^{-1}). The calculated diffusion coefficient in presence of 0.5 equiv of amine is 5.81 ×

10^{-6} cm^2s^{-1}, which decreases to 2.87×10^{-7} cm^2s^{-1} in case of **(16-A)$_2$-V^{2+}** at 11.5 mM.

Furthermore, the diffusion coefficient (D) is inversely proportional to the viscosity (η) of the medium as described by the Stokes–Einstein equation [Eq. (3)]:[42]

$$D = kT/6\pi\eta r \quad (3)$$

In this equation, D is the diffusion coefficient of the medium; k is the Boltzmann constant, T is the absolute temperature (K); η is the viscosity of the medium; r is the radius of the spherical particle.

On the basis of the Equations (2) and (3), the trend of decreased peak current can be rationalized as a consequence of the increase in the viscosity of the medium (i_p is inversely proportional to η) with increasing amount of amine (**16-A**) in the mixture. This explanation is further supported by the rheology experiments (discussed below).

Figure 4c shows the complex impedance plots (Nyquist plot) recorded with **(16-A)$_n$-V^{2+}** at various acid (**V^{2+}**)-to-amine (**16-A**) ratios. The semicircle arc represents the CT resistance of the sample and the working electrode. A shorter diameter arc represents lower CT resistance and higher CT rate at the interface. It is quite evident from the Nyquist plots[44] that the CT resistance increases with an increased amount of amine (**16-A**) in **(16-A)$_n$-V^{2+}**, which reflects the superior CT capacity of the former over the other studied samples. The order of CT resistance is: [$n=2$, (583.07 Ω)] > [$n=1$, (178.85 Ω)] > [$n=0.5$, (112.31 Ω)] > [**V^{2+}** (74.01 Ω)]. Hence, this result clearly supports the findings obtained in the cyclic voltammetry experiment.

In **(16-A)$_2$-V^{2+}**, the amide functionality links the redox-active polar headgroup with the n-$C_{16}H_{33}$ chain. Interestingly, it was found that **(16-A)$_{1.5}$-V^{2+}** and **(16-A)$_2$-V^{2+}** were able to disperse pristine-SWNTs efficiently (Figure 5a and b). However, no dispersion could be achieved at the acid (**V^{2+}**)-to-amine (**16-A**) ratios of 1:0.5 and 1:1. Maximum dispersion was acquired for the acid (**V^{2+}**)/amine (**16-A**) stoichiometric ratio of 1:2. This phenomenon ascribes to the importance of two equivalents of **16-A** to satisfy the amphiphilic nature of the molecule.

The aqueous suspension of **(16-A)$_2$-V^2**–SWNTs was characterized by UV/Vis-NIR spectroscopy (Figure S6a in the Supporting Information). Debundled SWNTs afforded distinctive peaks associated with the first interband transitions for the metallic NTs, M_{11} (400–650 nm) and the first (S11, 900–1600 nm) and the second (S22, 550–900 nm) interband transitions for the semiconductor forms. These sharp van Hove peaks are a characteristic feature of debundled, individually dispersed SWNTs and indicate that **(16-A)$_2$-V^{2+}** has a remarkable ability to debundle SWNTs in water.[45] Moreover, a Raman spectrum ($\lambda_{ex}=$ 633 nm) of the sample evidenced a sharp peak, with a shoulder in the high frequency region of 1500–1600 cm^{-1} (G^+-band and G^--band; Figure S6b in the Supporting Information). The low-frequency range belongs to the radial breathing modes (RBM), for which frequencies are dependent on the diameter of the nanotubes.[45] The characteristic RBM bands at 190 and 210 cm^{-1} originated due to the presence of semiconducting and metallic SWNTs, respectively, where the intensities of the two bands are almost equal. This result indicates that **(16-A)$_2$-V^{2+}** solubilizes both the metallic and the semiconducting form of SWNTs.[46]

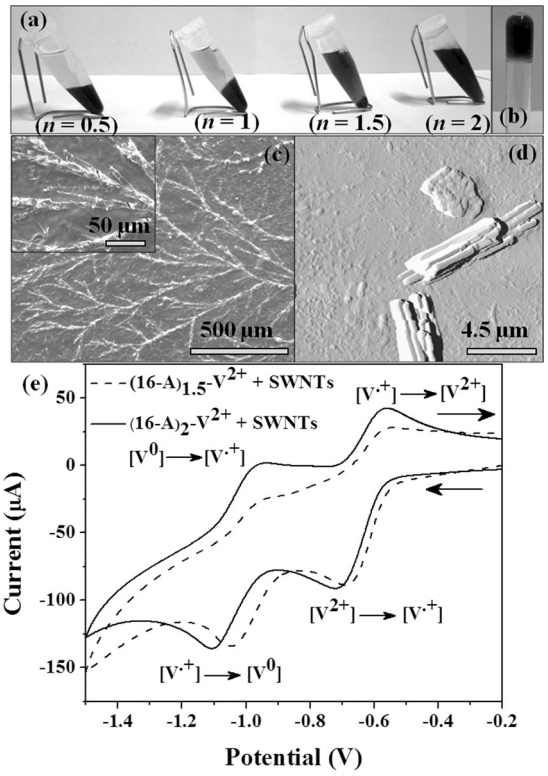

Figure 5. (a) Photographs of aqueous solutions of **(16-A)$_n$-V^{2+}** ($n=0.5$, 1, 1.5 and 2), showing different extent of solubilization of SWNTs in water at different acid (**V^{2+}**)/amine (**16-A**) stoichiometric ratios. The concentrations of **V^{2+}** and SWNTs are 5 mM and 0.25 mg mL^{-1}, respectively, in all cases. (b) Photograph of a typical SWNTs hydrogel composite of **(16-A)$_2$-V^{2+}**. The concentrations of **V^{2+}** and the SWNTs are 11.5 mM and 0.25 mg mL^{-1}, respectively. (c) SEM and (d) AFM images of the **(16-A)$_2$-V^{2+}**–SWNTs composite. The concentrations of **(16-A)$_2$-V^{2+}** and the SWNTs are 5 mM and 0.1 mg mL^{-1}, respectively, in all cases. (e) Cyclic voltammetry responses of the SWNTs composites of **(16-A)$_{1.5}$-V^{2+}** and **(16-A)$_2$-V^{2+}** in water on a glassy carbon electrode in the presence of LiCl (0.1 M) as the supporting electrolyte at a scan rate of 50 mV sec^{-1}. The concentrations of **V^{2+}** and the SWNTs are 11.5 mM and 0.25 mg mL^{-1}, respectively, in all cases (pH ca. 6.9).

The superstructures created by an aqueous dispersion of the nanocomposites of **(16-A)$_2$-V^{2+}**–SWNT were examined by SEM and AFM. Interestingly, the insertion of SWNTs in the self-assembly of **(16-A)$_2$-V^{2+}** did not change the basic morphological signatures of the self-assembled aggregates (Figure 5c). Fractured fibers were observed, probably due to the embedding of SWNTs inside the self-assembled **(16-A)$_2$-V^{2+}**. Results obtained from the AFM experiment were in good accordance with the SEM observations. **(16-A)$_2$-V^{2+}**–SWNTs composite in the aq. suspension exhibited broken bundle type of nanostructures (Figure 5d).

Figure 5e shows cyclic voltammograms of SWNTs composites of **(16-A)$_{1.5}$-V^{2+}** and **(16-A)$_2$-V^{2+}** in water. The concentration of the SWNTs is 0.25 mg mL^{-1} in each case. Interestingly, prominent peaks in the anodic scan appeared along with the

peaks in the cathodic scan (Table S4 in the Supporting Information). However, the peak-to-peak splitting (ΔE_p) is approximately 150 mV for both steps, which is larger than 59 mV (the required value for the reversible character of the system). The ratio i_{pa}/i_{pc} associated with the first half-wave potential is 0.35 for the **(16-A)$_{1.5}$-V^{2+}**–SWNTs composite and became almost 0.8 at a 1:2 acid (**V^{2+}**)/amine (**16-A**) stoichiometric ratio. Thus, insertion of SWNTs in **(16-A)$_2$-V^{2+}** transforms the electrochemically irreversible hydrogel to a quasi-reversible system.

Rheological behavior

Cyclic voltammetry studies have already demonstrated that increase in the amine (**16-A**) component resulted in a decrease of the peak current, which reached a minimum in **(16-A)$_2$-V^{2+}** due to the increase in the viscoelasticity of the resulting media. To probe this finding, rheological studies were performed to acquire valuable information pertaining to the correlation between the structure and the viscoelastic properties (Figure S7 in the Supporting Information). Figure S7a shows a comparison of the oscillatory frequency sweep response of **(16-A)$_n$-V^{2+}** at various acid (**V^{2+}**)/amine (**16-A**) stoichiometries. All the samples were subjected to frequency sweeps with a constant strain of 0.1%. G' and G'' from **(16-A)$_{1.5}$-V^{2+}** and **(16-A)$_2$-V^{2+}** remained independent of the frequency and the elastic modulus (G') was always greater than the associated loss modulus (G'') in the frequency range of 0.1–50 rad s^{-1}, thereby indicating the viscoelastic nature of these samples. However, G' and G'' from **(16-A)$_1$-V^{2+}** showed a different behavior compared with other mixtures of these two-components. At this ratio, G' and G'' showed an inclination to approach each other, and crossed over near 1 rad s^{-1}, eventually G'' became greater than G'. This behavior indicates a rather poor viscoelastic nature of the two-component self-assembly of **(16-A)$_1$-V^{2+}**.

Figure S7b shows the comparison of flow behavior of **(16-A)$_n$-V^{2+}** systems at different acid (**V^{2+}**)/amine (**16-A**) stoichiometric ratios. At a fixed applied frequency of 1 Hz, **(16-A)$_{1.5}$-V^{2+}** began to flow at approximately 29% critical strain, whereas **(16-A)$_2$-V^{2+}** at the identical concentration started to flow at a critical strain of about 48%, thus ascribing significantly higher viscoelastic, solidlike behavior of **(16-A)$_2$-V^{2+}** compared with that of **(16-A)$_{1.5}$-V^{2+}**.

Conclusions

In conclusion, we describe a novel supramolecular hydrogelation by mixing an *n*-$C_{16}H_{33}$-chain-appended L-alanine amphiphile (**16-A**) and a bis(carboxymethyl)-4,4′-bipyridinium salt (**V^{2+}**) in a 2:1 ratio. The role of salt (ion pair) formation on the self-assembly, leading to a lamellar-type of supramolecular organization, is reflected in the stoichiometry-dependent ^{1}H NMR and FT-IR spectroscopic results. SEM and AFM experiments reveal that these lamellar aggregates then lead to the formation of continuous 3D-fibrous networks, which act as hydrogel matrices that enable entrapment of water. Interestingly, the complexation of the dicarboxylic acid (**V^{2+}**) with the *n*-hexadecyl-chain-linked L-phenylalanine derivative (**16-F**) results in sol formation due to CT from the phenyl group of the L-phenylalanine to the viologen ring. The face-to-face stacking of the phenyl ring and the viologen ring as a consequence of CT interactions is manifested as distinct upfield shifts of the ^{1}H NMR signals, associated with both the phenyl and the viologen rings.

The redox activity of the hydrogel associated with the presence of the viologen moiety in **(16-A)$_2$-V^{2+}** has been demonstrated by stepwise $NaBH_4$ reduction, which induced gel-to-sol transition. Kaifer's group first established the concept that half-wave reduction potentials of the viologen core shift to more negative values with increased of size of the Newkome-type dendrimers, thus indicating an apparent thermodynamic hindrance for the reduction process for dendrimers with higher molecular mass. Herein, we demonstrate the utility of this concept for the first time in the supramolecular hydrogelation process. Half-wave reduction potentials of the viologen core of **(16-A)$_n$-V^{2+}** shift to more negative values with an increased proportion of the amine (**16-A**). Increment in the amine/acid stoichiometric ratio enhances the polarity of the environment around the viologen core; this in turn increases thermodynamic hindrance in the reduction process. In addition, it was possible to efficiently solubilize SWNTs in the hydrogel phase. An electrochemical analysis of the resultant nanocomposite unveiled that insertion of SWNTs converted the electrochemically irreversible hydrogel to a quasi-reversible system. To the best of our knowledge, this is the first report that shows such a remarkable electrochemical transition of an electroactive gel from irreversibility to quasi-reversibility by insertion of SWNTs. These interesting findings should be useful in developing novel electroactive nanocomposites for numerous applications in the near future.

Acknowledgements

We thank Prof. Narayan Pradhan, Mr. Biplab K. Patra, and Mr. Santimoy Khilari for assistance with the electrochemical experiments. This work was supported by the Department of Science and Technology, Government of India, New Delhi, India (J. C. Bose Fellowship to S.B.). S.D. thanks CSIR for a senior research fellowship.

Keywords: charge transfer · cyclic voltammetry · nanocomposite · redox-active hydrogel · self-assembly

[1] S. Datta, S. Bhattacharya, *Chem. Soc. Rev.* **2015**, *44*, 5596 – 5637.
[2] S. Bhattacharya, A. Srivastava, A. Pal, *Angew. Chem. Int. Ed.* **2006**, *45*, 2934 – 2937; *Angew. Chem.* **2006**, *118*, 3000 – 3003.
[3] A. R. Hirst, B. Escuder, J. F. Miravet, D. K. Smith, *Angew. Chem. Int. Ed.* **2008**, *47*, 8002 – 8018; *Angew. Chem.* **2008**, *120*, 8122 – 8139.
[4] a) X. Ma, H. Tian, *Acc. Chem. Res.* **2014**, *47*, 1971 – 1981; b) M. D. Segarra-Maset, V. J. Nebot, J. F. Miravet, B. Escuder, *Chem. Soc. Rev.* **2013**, *42*, 7086 – 7098; c) M. Nakahata, Y. Takashima, H. Yamaguchi, A. Harada, *Nat. Commun.* **2011**, *2*, 511; d) L. Hsu, G. L. Cvetanovich, S. I. Stupp, *J. Am. Chem. Soc.* **2008**, *130*, 3892 – 3899; e) A. Kishimura, T. Yamashita, T. Aida, *J. Am. Chem. Soc.* **2005**, *127*, 179 – 183.

[5] a) J. Nanda, A. Biswas, B. Adhikari, A. Banerjee, *Angew. Chem. Int. Ed.* **2013**, *52*, 5041 – 5045; *Angew. Chem.* **2013**, *125*, 5145 – 5149; b) A. Di Crescenzo, L. Bardini, B. Sinjari, T. Traini, L. Marinelli, M. Carraro, R. Germani, P. Di Profio, S. Caputi, A. Di Stefano, M. Bonchio, F. Paolucci, A. Fontana, *Chem. Eur. J.* **2013**, *19*, 16415 – 16423.

[6] S. Datta, S. K. Samanta, S. Bhattacharya, *Chem. Eur. J.* **2013**, *19*, 11364 – 11373.

[7] H. Shao, T. Nguyen, N. C. Romano, D. A. Modarelli, J. R. Parquette, *J. Am. Chem. Soc.* **2009**, *131*, 16374 – 16376.

[8] H. Shao, J. Seifert, N. C. Romano, M. Gao, J. J. Helmus, C. P. Jaroniec, D. A. Modarelli, J. R. Parquette, *Angew. Chem. Int. Ed.* **2010**, *49*, 7688 – 7691; *Angew. Chem.* **2010**, *122*, 7854 – 7857.

[9] J. H. Jung, G. John, K. Yoshida, T. Shimizu, *J. Am. Chem. Soc.* **2002**, *124*, 10674 – 10675.

[10] a) S. Datta, S. Bhattacharya, *Soft Matter* **2015**, *11*, 1945 – 1953; b) M. George, S. L. Snyder, P. Terech, C. J. Glinka, R. G. Weiss, *J. Am. Chem. Soc.* **2003**, *125*, 10275 – 10283.

[11] a) D. Mandal, S. K. Mandal, M. Ghosh, P. K. Das, *Chem. Eur. J.* **2015**, *21*, 12042 – 12052; b) R. Zou, Q. Wang, J. Wu, J. Wu, C. Schmuck, H. Tian, *Chem. Soc. Rev.* **2015**, *44*, 5200 – 5219; c) B. Adhikari, J. Nanda, A. Banerjee, *Chem. Eur. J.* **2011**, *17*, 11488 – 11496; d) Y. Gao, F. Zhao, Q. Wang, Y. Zhang, B. Xu, *Chem. Soc. Rev.* **2010**, *39*, 3425 – 3433; e) G. Palui, J. Nanda, S. Ray, A. Banerjee, *Chem. Eur. J.* **2009**, *15*, 6902 – 6909.

[12] a) D. K. Kumar, J. W. Steed, *Chem. Soc. Rev.* **2014**, *43*, 2080 – 2088; b) J. A. Foster, R. M. Edkins, G. J. Cameron, N. Colgin, K. Fucke, S. Ridgeway, A. G. Crawford, T. B. Marder, A. Beeby, S. L. Cobb, J. W. Steed, *Chem. Eur. J.* **2014**, *20*, 279 – 291; c) J. W. Steed, *Chem. Soc. Rev.* **2010**, *39*, 3686 – 3699.

[13] a) N. Yan, Z. Xu, K. K. Diehn, S. R. Raghavan, Y. Fang, R. G. Weiss, *J. Am. Chem. Soc.* **2013**, *135*, 8989 – 8999; b) S. R. Jadhav, P. K. Vemula, R. Kumar, S. R. Raghavan, G. John, *Angew. Chem. Int. Ed.* **2010**, *49*, 7695 – 7698; *Angew. Chem.* **2010**, *122*, 7861 – 7864; c) P. K. Vemula, J. Li, G. John, *J. Am. Chem. Soc.* **2006**, *128*, 8932 – 8938.

[14] a) A. Das, S. Ghosh, *Angew. Chem. Int. Ed.* **2014**, *53*, 2038 – 2054; *Angew. Chem.* **2014**, *126*, 2068 – 2084; b) M. Kumar, K. V. Rao, S. J. George, *Phys. Chem. Chem. Phys.* **2014**, *16*, 1300 – 1313; c) A. Das, M. Rahaman Molla, B. Maity, D. Koley, S. Ghosh, *Chem. Eur. J.* **2012**, *18*, 9849 – 9859.

[15] P. Dastidar, *Chem. Soc. Rev.* **2008**, *37*, 2699 – 2715.

[16] a) S. Datta, S. Bhattacharya, *Chem. Commun.* **2012**, *48*, 877 – 879; b) S. Kiyonaka, K. Sugiyasu, S. Shinkai, I. Hamachi, *J. Am. Chem. Soc.* **2002**, *124*, 10954 – 10955.

[17] D. Ke, C. Zhan, A. D. Q. Li, J. Yao, *Angew. Chem. Int. Ed.* **2011**, *50*, 3715 – 3719; *Angew. Chem.* **2011**, *123*, 3799 – 3803.

[18] a) W. Cao, X. Zhang, X. Miao, Z. Yang, H. Xu, *Angew. Chem. Int. Ed.* **2013**, *52*, 6233 – 6237; *Angew. Chem.* **2013**, *125*, 6353 – 6357; b) H.-Y. Lee, K. K. Diehn, K. Sun, T. Chen, S. R. Raghavan, *J. Am. Chem. Soc.* **2011**, *133*, 8461 – 8463; c) C. Wang, Q. Chen, F. Sun, D. Zhang, G. Zhang, Y. Huang, R. Zhao, D. Zhu, *J. Am. Chem. Soc.* **2010**, *132*, 3092 – 3096; d) K. Sun, R. Kumar, D. E. Falvey, S. R. Raghavan, *J. Am. Chem. Soc.* **2009**, *131*, 7135 – 7141.

[19] a) H. Komatsu, S. Matsumoto, S.-i. Tamaru, K. Kaneko, M. Ikeda, I. Hamachi, *J. Am. Chem. Soc.* **2009**, *131*, 5580 – 5585; b) S. Guha, M. G. B. Drew, A. Banerjee, *Chem. Mater.* **2008**, *20*, 2282 – 2290.

[20] a) L. Chen, K. S. Mali, S. R. Puniredd, M. Baumgarten, K. Parvez, W. Pisula, S. D. Feyter, K. Müllen, *J. Am. Chem. Soc.* **2013**, *135*, 13531 – 13537; b) X. Miao, W. Cao, W. Zheng, J. Wang, X. Zhang, J. Gao, C. Yang, D. Kong, H. Xu, L. Wang, Z. Yang, *Angew. Chem. Int. Ed.* **2013**, *52*, 7781 – 7785; *Angew. Chem.* **2013**, *125*, 7935 – 7939; c) C. J. Bowerman, B. L. Nilsson, *J. Am. Chem. Soc.* **2010**, *132*, 9526 – 9527; d) E. Krieg, E. Shirman, H. Weissman, E. Shimoni, S. G. Wolf, I. Pinkas, B. Rybtchinski, *J. Am. Chem. Soc.* **2009**, *131*, 14365 – 14373.

[21] Z. Yang, G. Liang, B. Xu, *Acc. Chem. Res.* **2008**, *41*, 315 – 326.

[22] Y.-L. Zhao, I. Aprahamian, A. Trabolsi, N. Erina, J. F. Stoddart, *J. Am. Chem. Soc.* **2008**, *130*, 6348 – 6350.

[23] a) S. Datta, S. Bhattacharya, *Chem. Commun.* **2015**, *51*, 13929 – 13932; b) S. Yamaguchi, I. Yoshimura, T. Kohira, S.-i. Tamaru, I. Hamachi, *J. Am. Chem. Soc.* **2005**, *127*, 11835 – 11841.

[24] a) X. Yang, G. Zhang, D. Zhang, *J. Mater. Chem.* **2012**, *22*, 38 – 50; b) W. R. Browne, B. L. Feringa, *Chimia* **2010**, *64*, 398 – 403; c) W. R. Browne, M. M. Pollard, B. de Lange, A. Meetsma, B. L. Feringa, *J. Am. Chem. Soc.* **2006**, *128*, 12412 – 12413.

[25] a) Y. Liu, W. Lei, T. Chen, L. Jin, G. Sun, B. Yin, *Chem. Eur. J.* **2015**, *21*, 15235 – 15245; b) C. Wang, F. Sun, D. Zhang, G. Zhang, D. Zhu, *Chin. J. Chem.* **2010**, *28*, 622 – 626; c) J. Puigmartí-Luis, E. E. Laukhina, V. N. Laukhin, A. P. del Pino, N. Mestres, J. Vidal-Gancedo, C. Rovira, D. B. Amabilino, *Adv. Funct. Mater.* **2009**, *19*, 934 – 941; d) X. Yang, G. Zhang, L. Li, D. Zhang, L. Chi, D. Zhu, *Small* **2012**, *8*, 578 – 584; e) J. Liu, J. Yan, X. Yuan, K. Liu, J. Peng, Y. Fang, *J. Colloid Interface Sci.* **2008**, *318*, 397 – 404; f) J. Puigmartí-Luis, V. Laukhin, A. P. del Pino, J. Vidal-Gancedo, C. Rovira, E. Laukhina, D. B. Amabilino, *Angew. Chem. Int. Ed.* **2007**, *46*, 238 – 241; *Angew. Chem.* **2007**, *119*, 242 – 245; g) C. Wang, D. Zhang, D. Zhu, *J. Am. Chem. Soc.* **2005**, *127*, 16372 – 16373; h) T. Kitahara, M. Shirakawa, S.-i. Kawano, U. Beginn, N. Fujita, S. Shinkai, *J. Am. Chem. Soc.* **2005**, *127*, 14980 – 14981; i) T. Akutagawa, K. Kakiuchi, T. Hasegawa, S.-i. Noro, T. Nakamura, H. Hasegawa, S. Mashiko, J. Becher, *Angew. Chem. Int. Ed.* **2005**, *44*, 7283 – 7287; *Angew. Chem.* **2005**, *117*, 7449 – 7453; j) T. Kitamura, S. Nakaso, N. Mizoshita, Y. Tochigi, T. Shimomura, M. Moriyama, K. Ito, T. Kato, *J. Am. Chem. Soc.* **2005**, *127*, 14769 – 14775.

[26] S. Kawano, N. Fujita, S. Shinkai, *J. Am. Chem. Soc.* **2004**, *126*, 8592 – 8593.

[27] a) R. Afrasiabi, H.-B. Kraatz, *Chem. Eur. J.* **2015**, *21*, 7695 – 7700; b) B. Adhikari, C. Singh, A. Shah, A. J. Lough, H.-B. Kraatz, *Chem. Eur. J.* **2015**, *21*, 11560 – 11572; c) B. Adhikari, H.-B. Kraatz, *Chem. Commun.* **2014**, *50*, 5551 – 5553; d) N. V. Lakshmi, D. Mandal, S. Ghosh, E. Prasad, *Chem. Eur. J.* **2014**, *20*, 9002 – 9011; e) R. Afrasiabi, H.-B. Kraatz, *Chem. Eur. J.* **2013**, *19*, 17296 – 17300; f) J. Liu, P. L. He, J. L. Yan, X. H. Fang, J. X. Peng, K. Q. Liu, Y. Fang, *Adv. Mater.* **2008**, *20*, 2508 – 2511.

[28] Y. Zhang, B. Zhang, Y. Kuang, Y. Gao, J. Shi, X. X. Zhang, B. Xu, *J. Am. Chem. Soc.* **2013**, *135*, 5008 – 5011.

[29] a) Z. Sun, Q. Huang, T. He, Z. Li, Y. Zhang, L. Yi, *ChemPhysChem* **2014**, *15*, 2421 – 2430; b) Z. Sun, Z. Li, Y. He, R. Shen, L. Deng, M. Yang, Y. Liang, Y. Zhang, *J. Am. Chem. Soc.* **2013**, *135*, 13379 – 13386.

[30] P. S. Kubiak, S. Awhida, C. Hotchen, W. Deng, B. Alston, T. O. McDonald, D. J. Adams, P. J. Cameron, *Chem. Commun.* **2015**, *51*, 10427 – 10430.

[31] a) M. Frasconi, I. R. Fernando, Y. Wu, Z. Liu, W.-G. Liu, S. M. Dyar, G. Barin, M. R. Wasielewski, W. A. Goddard, III, J. F. Stoddart, *J. Am. Chem. Soc.* **2015**, *137*, 11057 – 11068; b) S. M. Kim, J. H. Jang, K. K. Kim, H. K. Park, J. J. Bae, W. J. Yu, I. H. Lee, G. Kim, D. D. Loc, U. J. Kim, E. H. Lee, H. J. Shin, J. Y. Choi, Y. H. Lee, *J. Am. Chem. Soc.* **2009**, *131*, 327 – 331.

[32] a) K.-P. Wang, Y. Chen, Y. Liu, *Chem. Commun.* **2015**, *51*, 1647 – 1649; b) Q. Zhang, D.-H. Qu, X. Ma, H. Tian, *Chem. Commun.* **2013**, *49*, 9800 – 9802; c) K. V. Rao, K. Jayaramulu, T. K. Maji, S. J. George, *Angew. Chem. Int. Ed.* **2010**, *49*, 4218 – 4222; *Angew. Chem.* **2010**, *122*, 4314 – 4318; d) Y. Liu, Y. Yu, J. Gao, Z. Wang, X. Zhang, *Angew. Chem. Int. Ed.* **2010**, *49*, 6576 – 6579; *Angew. Chem.* **2010**, *122*, 6726 – 6729.

[33] D. Tasis, N. Tagmatarchis, A. Bianco, M. Prato, *Chem. Rev.* **2006**, *106*, 1105 – 1136.

[34] T. Ogoshi, Y. Takashima, H. Yamaguchi, A. Harada, *J. Am. Chem. Soc.* **2007**, *129*, 4878 – 4879.

[35] M. Zheng, A. Jagota, E. D. Semke, B. A. Diner, R. S. McLean, S. R. Lustig, R. E. Richardson, N. G. Tassi, *Nat. Mater.* **2003**, *2*, 338 – 342.

[36] a) D. Mandal, T. Kar, P. K. Das, *Chem. Eur. J.* **2014**, *20*, 1349 – 1358; b) S. K. Mandal, T. Kar, P. K. Das, *Chem. Eur. J.* **2013**, *19*, 12486 – 12496; c) S. Brahmachari, D. Das, A. Shome, P. K. Das, *Angew. Chem. Int. Ed.* **2011**, *50*, 11243 – 11247; *Angew. Chem.* **2011**, *123*, 11439 – 11443; d) S. Roy, A. Baral, A. Banerjee, *Chem. Eur. J.* **2013**, *19*, 14950 – 14957.

[37] a) T. Fukushima, K. Asaka, A. Kosakaa, T. Aida, *Angew. Chem. Int. Ed.* **2005**, *44*, 2410 – 2413; *Angew. Chem.* **2005**, *117*, 2462 – 2465; b) T. Fukushima, A. Kosaka, Y. Ishimura, T. Yamamoto, T. Takigawa, N. Ishii, T. Aida, *Science* **2003**, *300*, 2072 – 2074.

[38] A. Pal, B. S. Chhikara, A. Govindaraj, S. Bhattacharya, C. N. R. Rao, *J. Mater. Chem.* **2008**, *18*, 2593 – 2600.

[39] S. Samanta, A. Pal, S. Bhattacharya, C. N. R. Rao, *J. Mater. Chem.* **2010**, *20*, 6881 – 6890; S. Samanta, A. Pal, S. Bhattacharya, *Langmuir* **2009**, *25*, 8567 – 8578.

[40] a) M. E. Bush, N. D. Bouley, A. R. Urbach, *J. Am. Chem. Soc.* **2005**, *127*, 14511 – 14517; b) A. S. Jalilov, S. Patwardhan, A. Singh, T. Simeon, A. A. Sarjeant, G. C. Schatz, F. D. Lewis, *J. Phys. Chem. B* **2014**, *118*, 125 – 133.

[41] a) A. Pal, H. Basit, S. Sen, V. K. Aswal, S. Bhattacharya, *J. Mater. Chem.* **2009**, *19*, 4325 – 4334; b) H. Basit, A. Pal, S. Sen, S. Bhattacharya, *Chem. Eur. J.* **2008**, *14*, 6534 – 6545.

[42] a) W. Ong, A. Kaifer, *J. Am. Chem. Soc.* **2002**, *124*, 9358 – 9359; b) C. Cardona, A. Kaifer, *J. Am. Chem. Soc.* **1998**, *120*, 4023 – 4024.
[43] a) D. Podkoscielny, S. Gadde, A. Kaifer, *J. Am. Chem. Soc.* **2009**, *131*, 12876 – 12877; b) W. Wang, A. Kaifer, *Angew. Chem. Int. Ed.* **2006**, *45*, 7042 – 7046; *Angew. Chem.* **2006**, *118*, 7200 – 7204; c) W. Ong, J. Grindstaff, D. Sobransingh, R. Toba, J. M. Quintela, C. Peinador, A. Kaifer, *J. Am. Chem. Soc.* **2005**, *127*, 3353 – 3361; d) W. Ong, A. Kaifer, *Angew. Chem. Int. Ed.* **2003**, *42*, 2164 – 2167; *Angew. Chem.* **2003**, *115*, 2214 – 2217; e) I. Philip, A. Kaifer, *J. Am. Chem. Soc.* **2002**, *124*, 12678 – 12679.
[44] S. Khilari, S. Pandit, J. L. Varanasi, D. Das, D. Pradhan, *ACS Appl. Mater. Interfaces* **2015**, *7*, 20657 – 20666.
[45] a) S. K. Mandal, T. Kar, D. Das, P. K. Das, *Chem. Commun.* **2012**, *48*, 1814 – 1816; b) K. Nobusawa, A. Ikeda, J. Kikuchi, S. Kawano, N. Fujita, S. Shinkai, *Angew. Chem. Int. Ed.* **2008**, *47*, 4577 – 4580; *Angew. Chem.* **2008**, *120*, 4653 – 4656.
[46] a) B. Maji, S. K. Samanta, S. Bhattacharya, *Nanoscale* **2014**, *6*, 3721 – 3730; b) H. Kataura, Y. Kumazawa, Y. Maniwa, I. Umezu, S. Suzuki, Y. Ohtsuka, Y. Achiba, *Synth. Met.* **1999**, *103*, 2555 – 2558.

Received: January 16, 2016
Published online on April 5, 2016